Springer / Electrical Engineering
The final publication is available at https://doi.org/10.1007/s00202-018-0701-0

Magnetic Equivalent Circuit of MF Transformers: Modeling and Parameters Uncertainties

Thomas Guillod · Florian Krismer · Johann W. Kolar

Received: 9 November 2017 / Accepted: 17 May 2018

Abstract Medium-Frequency (MF) transformers are extensively used in power electronic converters. Accordingly, accurate models of such devices are required, especially for the magnetic equivalent circuit. Literature documents many different methods to calculate the magnetizing and leakage inductances of transformers, where, however, few comparisons exist between the methods. Furthermore, the impact of underlying hypotheses and parameter uncertainties is usually neglected. This paper analyzes nine different models, ranging from simple analytical expressions to 3D detailed numerical simulations. The accuracy of the different methods is assessed by means of Monte-Carlo simulations and linearized statistical models. The experimental results, conducted with a 100 kHz / 20 kW MF transformer employed in a 400 V DC distribution system isolation, are in agreement with the simulations (below 14 % inaccuracy for all the considered methods). It is concluded that, considering typical tolerances, analytical models are accurate enough for most applications and that the tolerance analysis can be conducted with linearized models.

Keywords Power Electronics, Medium-Frequency Transformers, Equivalent Circuit, Leakage, Magnetizing, Finite Element Method, Measurement, Uncertainty, Tolerance, Monte-Carlo Simulation

1 Introduction

Many power electronic converters feature MF transformers for voltage transformation, impedance matching, and galvanic isolation [1–4]. MF transformers are combining high efficiency, high power density, and fast dynamic. The analysis of such devices can be split into several categories:

Thomas Guillod (0000-0003-0738-5823)

E-mail: guillod@lem.ee.ethz.ch
Phone: +41 44 632 42 67
Power Electronic Systems Laboratory
ETH Zürich, Switzerland

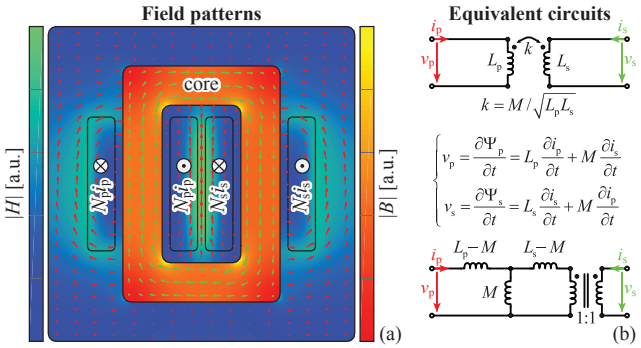

Fig. 1 (a) Core-type transformer field patterns during rated operating condition: magnetic flux density inside the core (magnetizing flux) and magnetic field in the winding window (leakage flux). (b) Inductance matrix with the corresponding (lossless) linear equivalent circuits.

- *Magnetic:* A magnetic equivalent circuit is usually used to describe the magnetizing flux, the leakage flux, and the voltage transfer ratio of a transformer [5–7].
- *Electric:* The electric field computation allows the extraction of the parasitic capacitances and the insulation coordination [4, 8].
- *Losses:* Different methods exist for computing the winding losses at MF (e.g. due to skin and proximity effects) [6, 9] and the core losses (e.g. due to hysteresis and eddy current losses) [6, 10]. Additionally, the losses in the cooling system [1], the losses inside shielding elements [4], and the dielectric losses [8] can be significant for some designs.
- *Thermal:* A thermal model of the transformer and the corresponding cooling system is used for the extraction of the temperature distribution [1, 6].

These different categories are physically interconnected and it appears that the extraction of the magnetic parameters is particularly important for determining the applied currents, the losses, parasitic resonances, etc.

Fig. 1(a) illustrates the different magnetic fluxes, which are defining the flux linkages of a transformer. The resulting inductance matrix, cf. Fig. 1(b), can be expressed with equivalent circuits, which are analyzed in detail in

Appendix A. Typically, the following magnetic parameters are used to characterize a transformer [6, 11]:

- *Voltage transfer ratio:* The voltage transfer ratio is the ratio between the primary and secondary voltages of a transformer. For a transformer with a high magnetic coupling factor, the voltage transfer ratio is almost equal to the turns ratio and load independent (near the nominal load).
- *Transformer magnetization:* A magnetizing current is required for generating the flux inside the core of the transformer (cf. Fig. 1(a)). The magnetizing current is related to the open-circuit inductances (self-inductances) of the transformer, which are measured from the primary and secondary sides. The open-circuit inductances are important for determining the core losses and the saturation current [12]. The magnetizing current can also be used for the converter operation, typically for achieving Zero-Voltage Switching (ZVS) [4, 13].
- *Transformer leakage:* The leakage flux is the magnetic flux which does not contribute to the magnetic coupling between the windings (cf. Fig. 1(a)). For a transformer with a high magnetic coupling factor, the leakage flux is related to the short-circuit inductances, which are measured from the primary and secondary sides. The short-circuit inductances are important for determining the winding losses and the short-circuit impedance of the transformer [5]. Moreover, the short-circuit inductances can be used as a series inductor for the power converter operation [14, 15].

Therefore, the extraction of an accurate equivalent circuit is critical for the design and optimization of transformers. Inaccurate values can lead to increased losses [1, 16] or to improper converter operation [17]. The magnetic parameters of the transformer can also be used for diagnosis (production and aging) [18]. This indicates that the selection of the most suitable (concerning accuracy, modeling cost, and computational cost) computation method for the equivalent circuit is a challenging and important task.

Literature identifies different methods for the computation of the equivalent circuit inductances: approximations of the air gap fringing field [6, 12, 19, 20], core reluctance computation [5, 6], analytical computation of the leakage field [5, 6, 21–23], semi-analytical computation of the leakage field [5, 7], and numerical simulations of the magnetic field distribution [5, 21, 24]. A detailed review of the existing methods can be found in [25, 26].

Nevertheless, deviations between the measured values and the expected values can arise from model inaccuracies, geometrical tolerances, material parameter tolerances, and measurement uncertainties. However, only few comparisons between the methods can be found [25, 27], where the impact of tolerances and uncertainties is ignored.

Table 1 MF Transformer Parameters.

Parameter	Value
Power	$P = 20.0\,\text{kW}$ / $S = 22.8\,\text{kVA}$
Excitation	400 V (DC-links) / 57 A (RMS) / 100 kHz
Windings	6 : 6 shell-type / 2500 × 100 µm HF litz wire
Insulation	Mylar / 1 kV (RMS, CM) / 1 kV (RMS, DM)
Core	4 × E80/38/20 / ferrite / TDK N87 material
Air gaps	2 × 0.7 mm (geometry) / 1.4 mm (magnetic)
Terminations	2 × 220 mm (parallel wires)
Volume / weight	80 mm × 82 mm × 154 mm / 1.0 dm^3 / 2.4 kg
Performance	99.65 % @ 20 kW / 99.60 % @ 10 kW

This paper analyzes the impact of tolerances on the magnetic equivalent circuit of MF transformers, which are employed in higher power (several 1 kW to several 100 kW) converter systems, for different computation methods. Section 2 defines the parameters of the considered 100 kHz / 20 kW MF transformer. Section 3 discusses nine different models for computing the magnetic parameters: standard analytical methods (e.g. Rogowski and McLyman factors) [6, 12, 22], more elaborate semi-analytical methods (e.g. Schwarz-Christoffel mapping, mirroring method) [5, 7, 19], and Finite Element Method (FEM) models (2D and 3D models with different levels of detail). Section 4 summarizes two approaches (Monte-Carlo simulations and linearized statistical models) for assessing the impact of tolerances on the equivalent circuit. Finally, Section 5 presents simulation and measurement results for the considered MF transformer, which concludes that simple analytical methods are very accurate and that linearized tolerance analyses are valid.

2 Considered Transformer

Fig. 2(a) depicts the considered 400 V / 100 kHz / 20 kW DC-DC series-resonant LLC converter. This converter provides a galvanic isolation for a section of a 400 V DC distribution grid, e.g. for the next generation datacenters [28, 29]. The converter is operated at the resonance frequency with 50 % duty cycle and acts as a "DC transformer", i.e. advantageously provides voltage transformation nearly independently of the load conditions [14].

Fig. 2(b) shows the considered MF transformer equivalent circuit and the corresponding short-circuit and open-circuit inductances. The leakage inductance of the MF transformer is part of the converter resonant tank [14, 15] and the magnetizing inductance is used for achieving ZVS [13, 30]. Fig. 2(c) shows the voltage and current waveforms applied to the MF transformer. Since the leakage and magnetizing inductances of the MF transformer are actively used for the converter operation, any mismatch

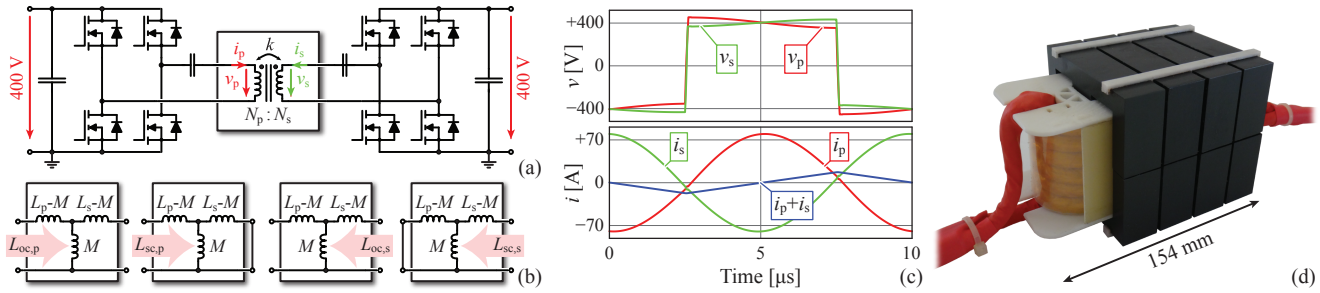

Fig. 2 (a) Considered 400 V / 100 kHz / 20 kW DC-DC series-resonant LLC converter. (b) MF transformer equivalent circuit with the definitions of the open-circuit and short-circuit inductances. (c) Voltage and current waveforms for operation at the resonance frequency, ensuring a nearly load independent voltage transfer ratio. (d) Constructed MF transformer prototype (cf. Tab. 1).

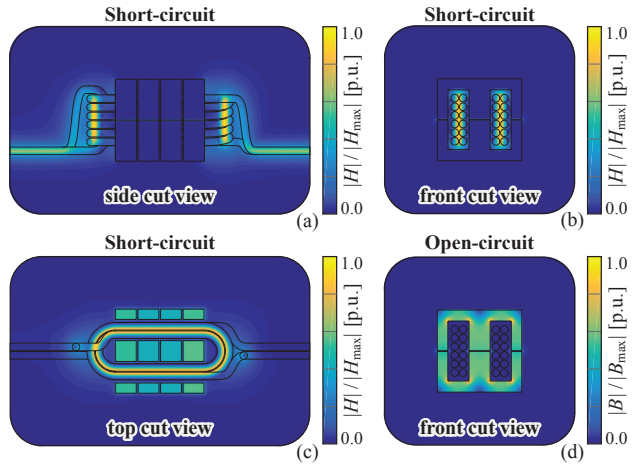

Fig. 3 (a) Side view, (b) front view, and (c) top view of the magnetic field during short-circuit operation. (d) Front view of the magnetic flux density during open-circuit operation. All the cut planes are intersecting at the MF transformer center point.

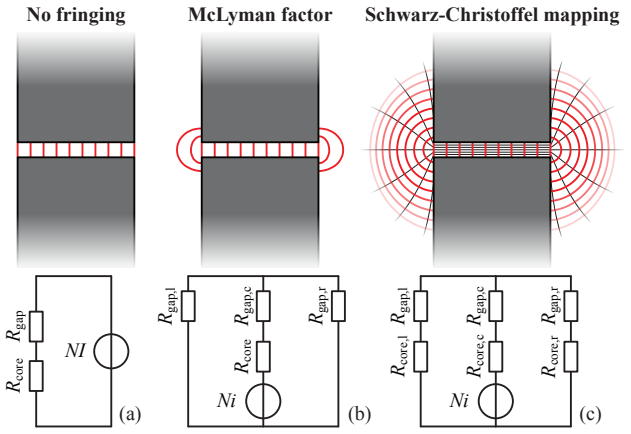

Fig. 4 Reluctance circuits (shown for E-shaped gapped core). (a) Single-element core model without fringing field model [6], (b) single-element core model with a semi-empirical fringing field model (McLyman factor) [12], and (c) detailed core model with a detailed fringing field model (Schwarz-Christoffel mapping) [5, 19]. The red lines indicate the direction of the magnetic flux density (streamlines).

between the measured and simulated values will lead to non-optimal operating conditions or will require an adaptation of the modulation scheme (e.g. dead times, switching frequency).

Fig. 2(d) depicts the constructed prototype and the key parameters are listed in Tab. 1. A large magnetizing current is required for achieving complete soft switching [13, 30]. Accordingly, two air gaps are introduced into the magnetic circuit, which, due to the associated fringing field, complicates the computation of the equivalent circuit. The air gaps also help the flux balancing between the paralleled core sets. Otherwise, this MF transformer features the most common design choices: E-shaped ferrite core, shell-type windings, and high-frequency (HF) litz wires [1–4]. However, the presented methods can also be adapted to designs employing nanocrystalline cores, core-type windings, solid wires, foil conductors, etc.

Fig. 3 shows the magnetic field and magnetic flux density during short-circuit and open-circuit operations. For short-circuit operation, the energy is mostly stored in the winding window and in the cable terminations. For open-circuit operation, the energy is stored in the air gaps and inside the core. This indicates that the considered MF transformer features a high magnetic coupling factor. In accordance, different methods can be used to extract the magnetic parameters of the transformer.

3 Computation Methods

The extraction of the equivalent circuit depicted in Fig. 1(b) is described in this Section for analytical, semi-analytical, and numerical methods. Additional information about the extraction of the equivalent circuit is given in Appendix B, Appendix C, and Appendix D.

3.1 Analytical Methods

Case: $i_p = 0 \vee i_s = 0$

First, the inductance is computed for the following operation condition: $i_p = 0 \vee i_s = 0$. This computation is similar to the computation of inductors, which implies that the

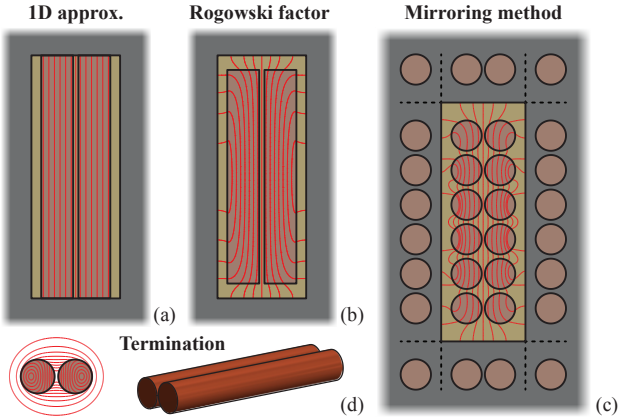

Fig. 5 Leakage magnetic field distribution (shown for a 6 : 6 shell-type windings). (a) 1D approximation (Ampère's circuital law) [6, 7], (b) 2D approximation of the field near the winding tips (Rogowski factor) [22], (c) 2D computation (mirroring method) [7, 31], and (d) cable termination field (Biot-Savart law). The red lines indicate the direction of the magnetic field (streamlines).

presented methods can also be applied to inductors. Most of the analytical methods are based on reluctance circuits:

- The core is modeled with a single reluctance and the fringing field of the air gaps is neglected (single equivalent reluctance), cf. Fig. 4(a) [6].
- The core is modeled with a single reluctance and the McLyman factor (simple semi-empirical model) is used for describing the fringing field of the air gaps, cf. Fig. 4(b) [12].
- The core is described with a detailed reluctance model (limbs, yokes, and corners) and a 3D model of the fringing field is used (based on Schwarz-Christoffel mapping), cf. Fig. 4(c) [5, 19]. However, the interactions between the different air gaps and the placement of the wires are not considered.

The main hypothesis of these reluctance models is that a perfect magnetic coupling between the turns composing a winding (same flux through all the turns) is given (cf. Fig. 3(d)). This implies that these computation methods are limited to transformers with high magnetic coupling factors. If required, the nonlinearities of the core material (flux density and frequency dependences) can be considered for the reluctance computations, especially for designs with small air gaps [12].

Case: $+N_\mathrm{p} i_\mathrm{p} = -N_\mathrm{s} i_\mathrm{s}$

In a second step, the inductance is computed for the following excitation: $+N_\mathrm{p} i_\mathrm{p} = -N_\mathrm{s} i_\mathrm{s}$. With this operating condition, most of the energy is stored in the winding window (cf. Fig. 3(b)) and the following computation methods can be used:

- A 1D approximation of the leakage field is computed with the Ampère's circuital law, cf. Fig. 5(a) [6, 7]. This model is inaccurate for windings with a low fill factor, for large distance between the windings and/or the core, and for modeling the leakage near the winding heads [7, 16].
- The 2D effects occurring near the winding tips, cf. Fig. 5(b) can be approximated with the Rogowki factor, which is a correction factor for the height of the windings [22].
- The 2D field distribution can be computed with the mirroring method (method of images) where the effect of the magnetic core is replaced by current images, cf. Fig. 5(c) [7, 31, 32]. The equivalent inductance can be extracted from the energy stored in the field [32], or, more conveniently, directly from the inductance matrix between the wires [33, 34]. The boundary conditions near the winding heads and the finite core permeability can be considered [7]. However, this method is only accurate if the leakage field can be approximated in 2D (cf. Figs. 3(b) and (c)).
- For a transformer with a reduced leakage inductance, the energy stored inside the cable terminations cannot be neglected [35]. For calculating the corresponding inductance, the inductance of two parallel wires (Biot-Savart law) can be used, cf. Fig. 5(d) [36]. Nevertheless, the field distribution near the cable terminations is intrinsically a 3D problem, which cannot be perfectly modeled analytically (cf. Fig. 3(a)).

If required, the aforementioned methods can be extended to other transformer geometries (e.g. core-type windings, three-phase windings, interleaved windings) [23] or for taking the frequency dependencies of the short-circuit inductances into account (especially for design with solid wires) [21].

Circuit Extraction

The equivalent circuit can be extracted from the obtained values ($i_\mathrm{p} = 0 \vee i_\mathrm{s} = 0$ and $+N_\mathrm{p} i_\mathrm{p} = -N_\mathrm{s} i_\mathrm{s}$) such that the energy stored in the equivalent circuit matches with the computed cases. This procedure is explained in detail in Appendix B. It should be noted that the analytical methods are inaccurate for transformers with low coupling factors ($k < 0.95$), where the aforementioned hypothesis (e.g reluctance circuit, energy distribution) are not valid anymore (cf. Appendix D).

3.2 FEM Simulations

Circuit extraction

The equivalent circuit of a transformer can also be obtained from numerical simulations, where FEM is typically selected [2–4, 37]. The exact geometry, the nonlinearities of the core material, and the frequency dependences of the current distribution (e.g. skin and proximity effects)

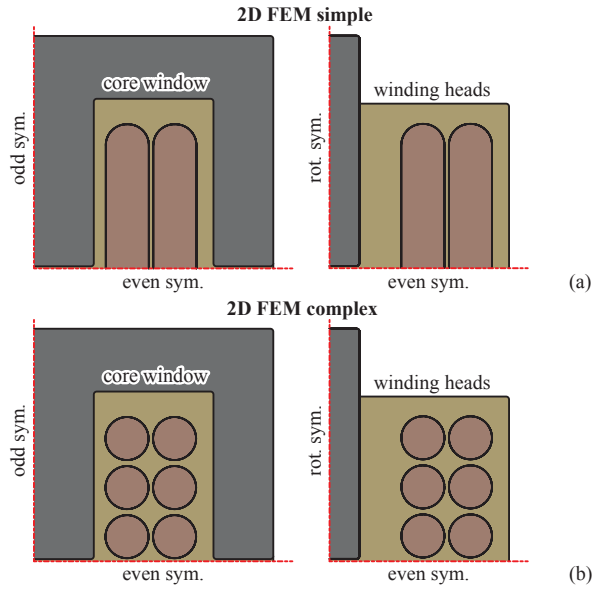

Fig. 6 (a) 2D FEM model with a simplified winding geometry and (b) with a detailed winding geometry. For both cases, a different model is used for the core window and the winding heads. The symmetry axes are also indicated.

can be represented. For extracting the equivalent circuit, which features three degrees of freedom, different simulations are required. In this paper, the extraction of the equivalent circuit is done with the following numerically stable procedure. The energy inside the system is extracted for the following cases: $i_\mathrm{p} \neq 0 \wedge i_\mathrm{s} = 0$ (energy in the primary self-inductance, L_p), $i_\mathrm{p} = 0 \wedge i_\mathrm{s} \neq 0$ (energy in the secondary self-inductance, L_s), and $+N_\mathrm{p} i_\mathrm{p} = -N_\mathrm{s} i_\mathrm{s}$ (approximately, for high magnetic coupling factors, the energy in the leakage magnetic field). Then, the equivalent circuit is determined such that the stored energy matches with the simulations (cf. Appendix C). This method is also applicable to transformers with low magnetic coupling factors.

2D Modeling

Fig. 6(a) depicts a 2D FEM model with a simplified winding structure and Fig. 6(b) considers the actual placement of the wires. For both cases, a planar and an axisymmetric model are used for modeling the core window and the winding heads, respectively (E-shaped core, shell-type windings). Different symmetry axes are used for reducing the size of the model.

3D Modeling

Fig. 7(a) shows a simple 3D model with simplified core and winding structures (single bodies). Fig. 7(b) considers the exact shape of the cores (core sets) and the different wires. These two models neglect the pitch of the windings and the cable terminations, such that different symmetry planes

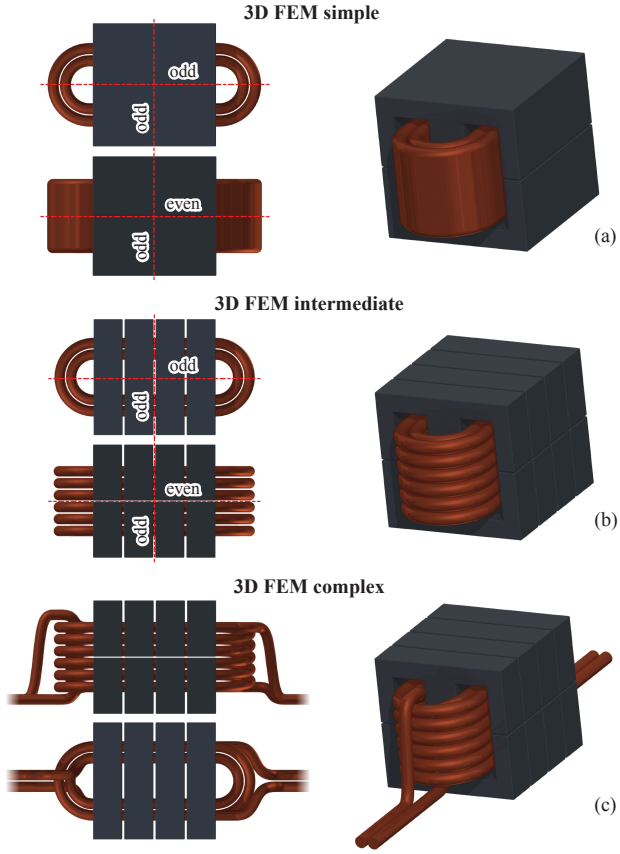

Fig. 7 (a) 3D FEM model with a simplified winding and core geometry, (b) with a more detailed winding and core geometry, and (c) with the actual transformer geometry (with the cable terminations). The considered symmetry planes are also indicated.

exist. Finally, Fig. 7(c) represents a full 3D model of the transformer and the cable terminations, which does not feature any symmetry plane.

4 Statistical Analysis

The aforementioned computation methods for the short-circuit ($L_\mathrm{sc,p}$ and $L_\mathrm{sc,s}$) and open-circuit ($L_\mathrm{oc,p}$ and $L_\mathrm{oc,s}$) inductances (cf. Fig. 2(b) and Section 3) are subject to the uncertainties of the used geometrical and material parameters. Therefore, the question arises if accurate calculations are actually necessary. However, the measurement of the uncertainties requires the construction of many identical transformers and, therefore, cannot be conducted during the design of a transformer. Accordingly, in the following, the tolerance analysis is conducted with the computation models.

4.1 Considered Parameters

The different uncertain parameters are named x_i, the tolerances $\pm\delta_i$, and the nominal values $x_{i,0}$. These parameters represent the uncertainties linked with the geometrical

Table 2 Uncertain Parameters (input).

Parameter	
n_x	Number of uncertain parameters
x_i	Uncertain value of the parameter
$x_{i,0}$	Nominal value of the parameter
$\pm\delta_i$	Tolerance around $x_{i,0}$
Worst-case analysis	
$f_{i,\mathrm{wc}}$	Probability density function (uniform distribution)
$\mathrm{MC}_{i,\mathrm{wc}}$	Monte-Carlo samples
Normal distribution analysis	
$f_{i,\mathrm{nd}}$	Probability density function (normal distribution)
$\sigma_{i,\mathrm{nd}}$	Standard deviation of $f_{i,\mathrm{nd}}$
$p_{i,\mathrm{nd}}$	Confidence interval for $\sigma_{i,\mathrm{nd}}$
$\mathrm{MC}_{i,\mathrm{nd}}$	Monte-Carlo samples

Table 3 Uncertain Parameters (output).

Inductance	
L	Uncertain value of the inductance
L_0	Nominal value of the inductance
F_L	Function describing the computation method
C_L	Computational cost of F_L
L_{meas}	Nominal value of the measured inductance
$\{L\}_{\mathrm{meas}}$	Measurement tolerance interval
Worst-case analysis	
$\pm\delta_{L,\mathrm{wc}}$	Tolerance around L_0 (linearized analysis)
$\mathrm{MC}_{L,\mathrm{wc}}$	Monte-Carlo samples
$\{L\}_{\mathrm{lin,wc}}$	Tolerance interval (linearized analysis)
$\{L\}_{\mathrm{MC,wc}}$	Tolerance interval (Monte-Carlo simulations)
Normal distribution analysis	
$f_{L,\mathrm{nd}}$	Probability density function (linearized analysis)
$\sigma_{L,\mathrm{nd}}$	Standard deviation of $f_{L,\mathrm{nd}}$ (linearized analysis)
$p_{L,\mathrm{nd}}$	Confidence interval for $\sigma_{L,\mathrm{nd}}$ (linearized analysis)
$\pm\delta_{L,\mathrm{nd}}$	Tolerance around L_0 (linearized analysis)
$\mathrm{MC}_{i,\mathrm{nd}}$	Monte-Carlo samples
$\{L\}_{\mathrm{lin,nd}}$	Tolerance interval (linearized analysis)
$\{L\}_{\mathrm{MC,nd}}$	Tolerance interval (Monte-Carlo simulations)

tolerances and the material parameter tolerances. For the statistical analysis, the following expressions are considered:

$$L = F_L(x_1, x_2, \ldots), \tag{1}$$

$$L_0 = F_L(x_{1,0}, x_{2,0}, \ldots), \tag{2}$$

where L is the computed inductance, L_0 the nominal value, and F_L the function describing the inductance computation method (cf. Section 3). Tab. 2 and Tab. 3 summarize the variables used to describe the uncertain input parameters and the inductances, respectively.

In the following, a simple exemplary function F_L is considered for explaining the tolerance stacking analysis. Afterward, in Section 5, the defined analysis framework is then used for analyzing the tolerances for the open-circuit and short-circuit inductances of the considered

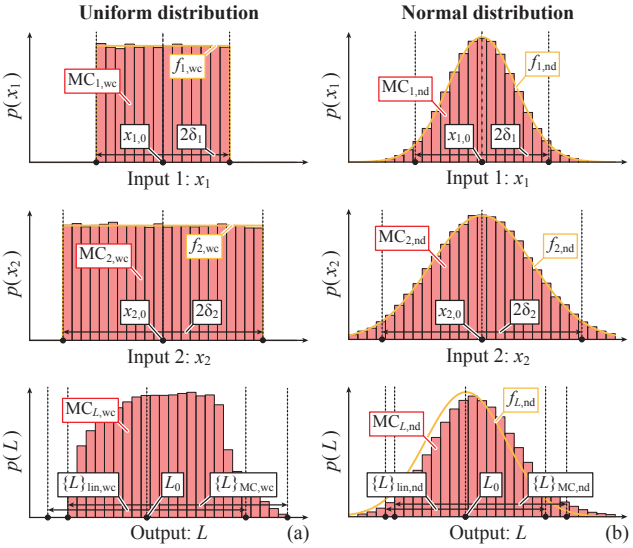

Fig. 8 (a) Worst-case analysis with uniform distributions. (b) Statistical analysis with normal distributions. Monte-Carlo simulations and linearized computations are compared. The following exemplary parameters are used: $n_x = 2$, $x_1 \pm \delta_1 = 0 \pm 1.0$, $x_2 \pm \delta_2 = 0 \pm 1.5$, $F_L = x_1 + ((x_2/2) - 0.2)^2$. The confidence intervals ($p_{i,\mathrm{nd}}$ and $p_{L,\mathrm{nd}}$) are set to 95 %. The number of Monte-Carlo samples is 10^4.

transformer (cf. Section 2), using the aforementioned computation methods (cf. Section 3).

4.2 Worst-Case Analysis

For a worst-case analysis, the variables x_i are assumed to be uniformly distributed in the tolerance intervals and independent of each other. The probability density distribution function, $f_{i,\mathrm{wc}}$, can be set to

$$f_{i,\mathrm{wc}}(x_i) = f_{\mathrm{uniform}}\left(x_i, x_{i,0} - \delta_i, x_{i,0} + \delta_i\right), \tag{3}$$

where f_{uniform} describes the probability density distribution function of the continuous uniform distribution. With the help of F_L (cf. (1)), the probability distribution of L can be computed and the extrema can be extracted, cf. Fig. 8(a).

For the magnetic equivalent circuit, many variables are present, F_L is nonlinear, and F_L, for some computation methods, cannot be expressed analytically. For these reasons, the probability density distribution function is obtained by means of Monte-Carlo simulations [38]. In the course of the Monte-Carlo simulations, a large number of random parameter combinations is generated with respect to the input probability distributions (cf. (3)) and the corresponding inductance values are computed. Then, it is straightforward to extract the interval, $\{L\}_{\mathrm{MC,wc}}$, where the inductance value is fluctuating.

However, Monte-Carlo simulations require the computation of a large number of designs. Alternatively, the function F_L can be linearized near the nominal values of

the different parameters, which leads to [39]

$$\delta_{L,\mathrm{wc}} = \sum_{i=1}^{n} \left| \left.\frac{\partial F_L}{\partial x_i}\right|_{x_{i,0}} \delta_i \right| \tag{4}$$

$$\{L\}_{\mathrm{lin,wc}} = [L_0 - \delta_{L,\mathrm{wc}}, L_0 + \delta_{L,\mathrm{wc}}], \tag{5}$$

where $\delta_{L,wc}$ is the obtained tolerance and $\{L\}_{\mathrm{lin,wc}}$ the corresponding interval. Beside the reduced computational cost, the linearization allows the analysis of the sensitivity of the inductance value with respect to the different parameters. If the linearization is valid, the ranges $\{L\}_{\mathrm{MC,wc}}$ and $\{L\}_{\mathrm{lin,wc}}$ should match together. In Fig. 8(a), some differences can be observed due to the strong nonlinearities of the considered exemplary function F_L.

4.3 Normal Distribution Analysis

The aforementioned worst-case analysis is often too conservative. For this reason, normal (Gaussian) distributions are often used for tolerance stacking analysis [39]. The probability density distribution function, $f_{i,\mathrm{nd}}$, and the standard deviation, $\sigma_{i,\mathrm{nd}}$, can be set to

$$f_{i,\mathrm{nd}}(x_i) = f_{\mathrm{normal}}\left(x_i, x_{i,0}, \sigma_{i,\mathrm{nd}}\right), \tag{6}$$

$$\sigma_{i,\mathrm{nd}} = \frac{\delta_i}{\sqrt{2}\mathrm{erf}^{-1}\left(p_{i,\mathrm{nd}}\right)}, \tag{7}$$

where f_{normal} is the probability density distribution function of the normal distribution and erf^{-1} the inverse Gauss error function [40]. The confidence intervals, $p_{i,\mathrm{nd}}$, are describing the percentage of the data lying within the accepted tolerances $\pm\delta_i$. With these definitions, the probability distribution of L can be computed, cf. Fig. 8(b).

Again, the probability density distribution function can be obtained by means of Monte-Carlo simulations, where the nonlinearities of F_L are considered [38]. The interval, where $p_{L,\mathrm{nd}}$ percent of the values are located (confidence interval), is depicted as $\{L\}_{\mathrm{MC,nd}}$.

Alternatively, the linearization of F_L can be conducted. A linear combination of normal distributions results in a normal distribution, which leads to

$$f_{L,\mathrm{nd}}(L) = f_{\mathrm{normal}}\left(L, L_0, \sigma_{L,\mathrm{nd}}\right), \tag{8}$$

$$\sigma_{L,\mathrm{nd}} = \sqrt{\sum_{i=1}^{n} \left(\left.\frac{\partial F_L}{\partial x_i}\right|_{x_{i,0}} \sigma_{i,\mathrm{nd}} \right)^2}, \tag{9}$$

where $f_{L,\mathrm{nd}}(L)$ is the probability density distribution function and $\sigma_{L,\mathrm{nd}}$ the standard deviation. With the confidence interval, $p_{L,\mathrm{nd}}$, the tolerance on the inductance value can be expressed as

$$\delta_{L,\mathrm{nd}} = \sigma_{L,\mathrm{nd}}\sqrt{2}\mathrm{erf}^{-1}\left(p_{L,\mathrm{nd}}\right), \tag{10}$$

$$\{L\}_{\mathrm{lin,nd}} = [L_0 - \delta_{L,\mathrm{nd}}, L_0 + \delta_{L,\mathrm{nd}}], \tag{11}$$

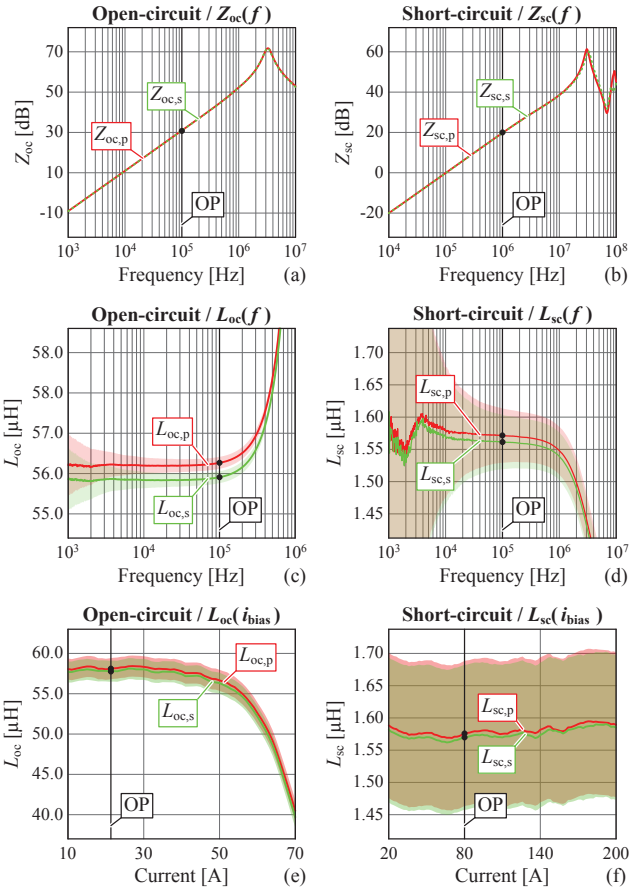

Fig. 9 (a) Measured open-circuit and (b) short-circuit impedances for the setup shown in Fig. 2(d) [41]. (c) Open-circuit and (d) short-circuit inductances for different frequencies [41]. (e) Open-circuit and (f) short-circuit small-signal differential inductances for different bias currents [42]. The primary and secondary windings are the outer and inner windings (with respect to the central limb), respectively. The measurement uncertainties (shaded area) and the operating points ("OP", cf. Fig. 2(c)) are indicated.

where $\delta_{L,nd}$ is the obtained tolerance and $\{L\}_{\mathrm{lin,nd}}$ the corresponding interval. In Fig. 8(b), the mismatch between the probability density distribution function obtained with Monte-Carlo simulations and $f_{L,\mathrm{nd}}(L)$ results from the nonlinearities of the chosen exemplary function F_L.

5 Results

The MF transformer depicted in Section 2 is considered. First the magnetic parameters of the MF transformer are measured. In a second step, the aforementioned computation methods (cf. Section 3) and tolerance stacking analysis (cf. Section 4) are applied. Finally, the measurement and computation results are compared.

5.1 Measurements

The open-circuit ($L_{\mathrm{oc,p}}$ and $L_{\mathrm{oc,s}}$) and short-circuit ($L_{\mathrm{sc,p}}$ and $L_{\mathrm{sc,s}}$) inductances (cf. Fig. 2(b)) are ex-

tracted from small-signal impedance measurements [43]. Figs. 9(a) and (b) depict the measured impedances, where the resonance frequencies of the MF transformer can be seen. Figs. 9(c) and (d) show the extracted nominal inductances (L_{meas}) with the corresponding measurement uncertainties ($\{L\}_{\text{meas}}$). The inductances are extracted with a resistive-inductive series equivalent circuit.

These measurements are obtained with an Agilent 4924A precision impedance analyzer [41]. The uncertainties are composed of the measurement device tolerances and an absolute error. The absolute error, which is estimated from measurements, is set to 20 nH for short-circuit measurements (interconnection inductances) and to 100 nH for open-circuit measurements (interconnection inductances and slight variation of the length of the air gaps in case the core halves are pressed together). These measurements have been successfully reproduced (less than 1 % deviation) with an Omicron Bode 100 network analyzer [44, 45].

Fig. 9(c) and (d) indicate that the frequency dependences of the inductances are negligible due to the used ferrite cores and HF litz wires [6, 21]. The slight increase of the open-circuit inductances near 1 MHz is due to the capacitive currents (resonance frequency of 3.2 MHz) [4]. The slight decrease of the short-circuit inductances near 10 MHz is explained by high-frequency effects (induced currents in the windings and permeability change of the core) [9, 21]. However, near the operating frequency (100 kHz), the impact of these high-frequency effects is negligible (constant open-circuit and short-circuit inductances below 1 MHz).

However, the MF transformer is not operated with small-signal excitations. For this reason, the MF transformer has also been measured with a ed-k DPG10/1000A power choke tester [42]. This device applies a current ramp to the MF transformer and measures the induced voltage. This enables the extraction of the small-signal differential inductance ($L = \partial\Psi/\partial i$) for different bias currents, cf. Figs. 9(e) and (f). The uncertainties are composed of the measurement device tolerances and an absolute error. The absolute error is set to 50 nH and 120 nH, respectively, for short-circuit (interconnection inductances) and open-circuit measurements (interconnection inductances and variation of the length of the air gaps).

Fig. 9(e) and (f) shows that the open-circuit inductances are also linear below 40 A (magnetizing current), which means that the MF transformer is operated well below the saturation (cf. Fig. 2(c)). As expected, the short-circuit inductances are independent of the current. Due to the high magnetic coupling factor of the MF transformer ($k = 0.986$), the inductances measured from the primary and secondary sides are very similar ($N_{\text{p}} = N_{\text{s}}$).

Table 4 Computation Methods.

Name	Model	C_L	n_x
Analytic simple	Figs. 4(a) / 5(a)	50 FLOPs	12
Analytic intermediate	Figs. 4(b) / 5(b)	150 FLOPs	14
Analytic complex	Figs. 4(c) / 5(c)	200 kFLOPs	16
Analytic termination	Figs. 4(c) / 5(c) / 5(d)	200 kFLOPs	20
2D FEM simple	Figs. 6(a) / 5(d)	8 kDOFs	19
2D FEM complex	Figs. 6(b) / 5(d)	12 kDOFs	20
3D FEM simple	Figs. 7(a) / 5(d)	0.9 MDOFs	17
3D FEM intermediate	Figs. 7(b) / 5(d)	1.4 MDOFs	17
3D FEM complex	Fig. 7(c)	7.2 MDOFs	16

For these reasons, the small-signal inductances ($i_{\text{bias}} = 0$ A) at the switching frequency ($f = 100$ kHz) are extracted for the comparison with the computations. Moreover, only the averages of the primary ($L_{\text{oc,p}}$ and $L_{\text{sc,p}}$) and secondary side inductances ($L_{\text{oc,p}}$ and $L_{\text{sc,p}}$) are further considered (called L_{oc} and L_{sc}, cf. Fig. 2(b)). The obtained nominal values (L_{meas}) and measurement uncertainties ($\{L\}_{\text{meas}}$) are used for comparing the measurement results with the different computation methods.

5.2 Computations

The computation methods described in Section 3 are combined, as shown in Tab. 4, for extracting the equivalent circuit of the MF transformer. For the analytical models, the computational cost, C_L, is measured in Floating Point Operations (FLOPs) [46]. For FEM models, the computational cost, C_L, is expressed in Degrees Of Freedom (DOFs) [37], given that three operating points are solved for extracting the equivalent circuit (cf. Subsection 3.2).

For the statistical analysis, the methods described in Section 4 are used. The confidence intervals for the parameters ($p_{i,\text{nd}}$) and for the inductances ($p_{L,\text{nd}}$) are set to 95 %. The number of uncertain parameters, n_x, is indicated in Tab. 4. The uncertain parameters can be classified into different categories:

- The geometrical and material tolerances are mostly extracted from the datasheets (e.g. core, coil former, and litz-wire). The uncertainties linked to the construction of the MF transformer (e.g. air gaps, insulation distances) are estimated. The main tolerances are the air gaps length ($0.7\,\text{mm} \pm 0.05\,\text{mm}$), the distance between the two windings ($0.75\,\text{mm} \pm 0.3\,\text{mm}$), the wire diameter ($7.2\,\text{mm} \pm 0.2\,\text{mm}$), the core permeability (2200 ± 500), and the core cross section ($1600\,\text{mm}^2 \pm 40\,\text{mm}^2$).
- Some geometrical parameter uncertainties are also linked to the geometrical approximations included in the modeling. The fact that a 3D geometry is modeled in 1D/2D (e.g. winding heads and cable terminations) introduces additional uncertainties since some geomet-

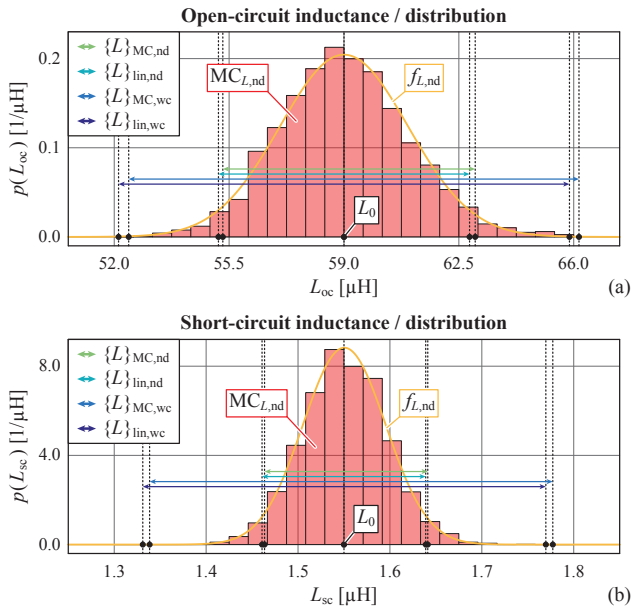

Fig. 10 (a) Tolerance analysis for the open-circuit and (b) short-circuit inductances. Worst-case and normal distribution analyzes are performed by means of Monte-Carlo simulations and linearization (cf. Section 4). The model "Analytic termination" is considered (cf. Tab. 4).

rical parameters in the 1D/2D models do not exist in the 3D models.

– The simplifications used in the different computation methods (e.g. 1D/2D modeling, no fringing field model, no cable terminations model) are intrinsic inaccuracies of the methods and, therefore, are not considered as uncertainties.

The computational cost of the FEM models is too high for Monte-Carlo simulations. On the other hand, the simple analytical models ("Analytic simple", "Analytic intermediate", and "Analytic complex") neglect many parameters (e.g. placement of the wires, cable terminations). Therefore, the full statistical analysis is performed with the model "Analytic termination", where 2×10^3 Monte-Carlo samples are considered.

Fig. 10 shows the obtained tolerances for the inductances, which are not negligible. It appears that the linearized statistical analysis is valid (compared to Monte-Carlo simulations). The linearized analysis allows the extraction of the sensitivities of the different parameters (cf. (4)), which is shown in Fig. 11. The main uncertainties are originating from the air gaps length, the size of the core, the permeability of the core, the insulation distances, and the simplification of the 3D geometry (depicted as "model approx.").

Therefore, the linearized statistical analysis is applied to all the computation methods described in Tab. 4. This greatly reduces the computational cost since only $2n_x + 1$ equivalent circuit computations are required. The obtained

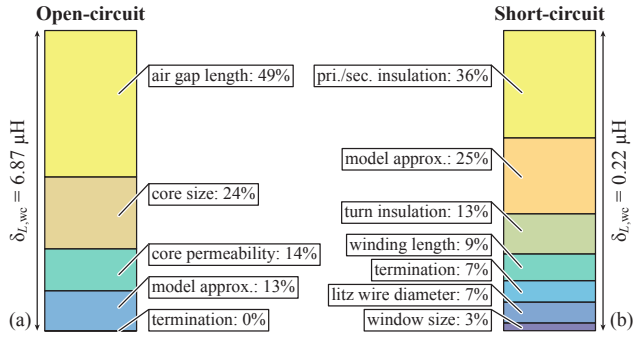

Fig. 11 (a) Sensitivity analysis for the open-circuit and (b) short-circuit inductances. The model "Analytic termination" is considered (cf. Tab. 4) and a linearized worst-case analysis is applied (cf. (4)).

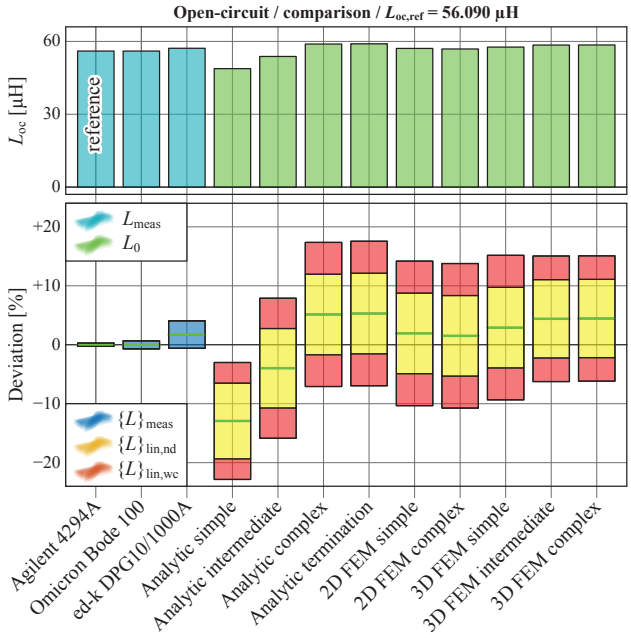

Fig. 12 Comparison between measurements (cf. Subsection 5.1) and computations (cf. Subsection 5.2) for the open-circuit inductance (L_{oc}). The reference value is the measurement obtained with an Agilent 4294A precision impedance analyzer [41].

values (L_0, $\{L\}_{\mathrm{lin,wc}}$, and $\{L\}_{\mathrm{lin,nd}}$) are used for comparing the computations and the measurements.

5.3 Comparison: Measurements and Computations

Fig. 12 and Fig. 13 show the comparison between measurements and computations for the open-circuit and short-circuit inductances, respectively. The most accurate measurements, i.e. the values obtained with the Agilent 4294A precision impedance analyzer [41], are selected as reference values for the extraction of the relative errors. The deviations between the nominal values and the reference value are smaller than 14 % for all the methods.

For the open-circuit inductance, the method "Analytic simple" (cf. Tab. 4) underestimates the inductance, which

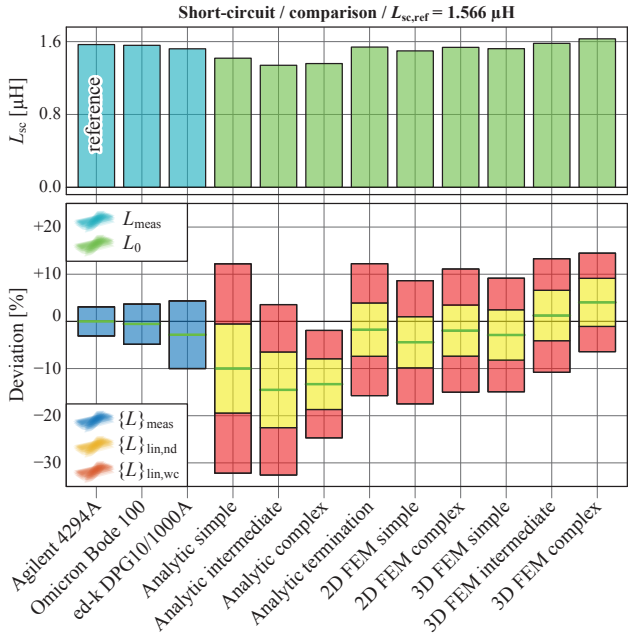

Fig. 13 Comparison between measurements (cf. Subsection 5.1) and computations (cf. Subsection 5.2) for the short-circuit inductance (L_{sc}). The reference value is the measurement obtained with an Agilent 4294A precision impedance analyzer [41].

is due to the neglected fringing field of the air gaps. For all the other methods, the tolerances ($\{L\}_{lin,wc}$ and $\{L\}_{lin,nd}$) match with the measurement uncertainties. The methods based on Schwarz-Christoffel mapping ("Analytic complex" and "Analytic termination") are in good agreement with the "3D FEM complex" method (1 % error).

For the short-circuit inductance, the methods which neglect the cable terminations ("Analytic simple", "Analytic intermediate", and "Analytic complex") underestimate the inductance. For all the other methods, the tolerances ($\{L\}_{lin,wc}$ and $\{L\}_{lin,nd}$) match with the measurement uncertainties. The method "Analytic termination" is also in good agreement with the "3D FEM complex" method (5 % error).

Therefore, it can be concluded that the complex computation methods (2D and 3D FEM models) only feature limited advantages over the analytical methods. The main advantage of the 3D FEM methods is a slight reduction of the tolerances, since the tolerances linked with the model approximations vanish ("model approx.", cf. Fig. 11). The method "Analytic termination" (cf. Tab. 4) represents an interesting trade-off between modeling complexity, computational cost, and accuracy.

It also appears that the measurement uncertainties are smaller than the computation tolerances. Furthermore, the deviation between the nominal value of the computation methods is smaller than the tolerances. This implies that the extraction of MF transformer equivalent circuit parameters can only be marginally improved with new computation and measurement methods. Only a reduction of the uncertainties on the geometry and material parameters will lead to better matching between measurements and computations.

6 Conclusion

This paper first investigates various computation methods for extracting MF transformer magnetic equivalent circuit, which is a critical parameter for the modeling and optimization of power electronic converters. Analytical models are presented for the magnetizing (reluctance circuit, Rogowski factor, and Schwarz-Christoffel mapping) and leakage (1D Ampère's circuital law, Rogowski factor, 2D mirroring method, and cable termination model) inductances. The advantages and limitations of the analytical methods are discussed and compared to numerical simulations (2D and 3D FEM).

In a next step, the uncertainties linked to model inaccuracies, geometrical tolerances, and material tolerances are analyzed in detail with a statistical analysis applied to the computation models. Computationally intensive Monte-Carlo simulations and simple linearized statistical models, which allow the analysis of the sensitivities for the different parameters, are considered.

The presented methods are finally applied for calculating the short-circuit and open-circuit inductances of a 100 kHz / 20 kW MF transformer. It is concluded that a linearized statistical analysis is sufficient, which greatly simplifies the tolerance analysis. The deviations between the measurements and the different computations methods can be explained with the computed tolerances. For the open-circuit inductance, the measurement uncertainties (0.3 – 2.3 %) are smaller than the computation tolerances (6 – 12 %). This is also the case for the short-circuit inductance (2.7 – 7.1 % and 5 – 22 %).

A comparison between the different computation methods shows that the combination of a reluctance circuit, Schwarz-Christoffel mapping, the mirroring method, and a cable termination model is a good trade-off between the computational cost and the obtained accuracy. Finally, it is concluded that the consideration of the uncertainties is required for improving the modeling of MF transformers. Moreover, the obtained uncertainties are also useful for production diagnosis and for selecting the right margin of safety during the design process.

The presented statistical analysis has been conducted on the magnetic parameters of MF transformers with computational models. This work could be completed with an experimental study involving many samples in order to measure the tolerances occurring in a typical production process. Furthermore, the presented methods can be extended to the remaining transformer parameters (e.g. losses and thermal models) and components

(e.g. switches, inductors) in order to assess the model uncertainties of complete converter systems.

Appendices

These appendices review the theoretical background behind the different transformer equivalent circuits and the corresponding pitfalls (cf. Appendix A). The procedure for extracting equivalent circuits from analytical (cf. Appendix B) and numerical (cf. Appendix C) computation is also presented. Finally, some approximations are given for transformers with high magnetic coupling factors (cf. Appendix D).

A Transformer Equivalent Circuits

The magnetic equivalent circuit of a (lossless) linear transformer with two windings is fully described by the following inductance matrix (cf. Fig. 1(b)) [6, 11, 43]:

$$\begin{bmatrix} v_\mathrm{p} \\ v_\mathrm{s} \end{bmatrix} = \begin{bmatrix} \frac{\partial \Psi_\mathrm{p}}{\partial t} \\ \frac{\partial \Psi_\mathrm{s}}{\partial t} \end{bmatrix} = \begin{bmatrix} L_\mathrm{p} & M \\ M & L_\mathrm{s} \end{bmatrix} \begin{bmatrix} \frac{\partial i_\mathrm{p}}{\partial t} \\ \frac{\partial i_\mathrm{s}}{\partial t} \end{bmatrix}, \tag{12}$$

where L_p is the primary self-inductance, L_s the secondary self-inductance, and M the mutual inductance. The inductance matrix features three independent parameters. The energy, W, stored in the transformer (quadratic form of the inductance matrix) can be computed as

$$W = \frac{1}{2} L_\mathrm{p} i_\mathrm{p}^2 + \frac{1}{2} L_\mathrm{s} i_\mathrm{s}^2 + M i_\mathrm{p} i_\mathrm{s}. \tag{13}$$

The energy stored in the transformer is always positive (i.e. the inductance matrix is positive definite), which leads to the condition $M^2 < L_\mathrm{p} L_\mathrm{s}$. Therefore, the mutual inductance can be expressed with a normalized parameter, the magnetic coupling,

$$k = \frac{M}{\sqrt{L_\mathrm{p} L_\mathrm{s}}}, \qquad \text{with } k \in [0,1]. \tag{14}$$

During open-circuit operation, the inductance matrix has the following physical interpretation. The self-inductances (L_p and L_s) represent flux linkages of the two windings themselves (defined as magnetizing flux linkages). The mutual inductance (M) describes the flux linkage between the windings (defined as coupled flux linkages). The differences between the self and mutual inductances ($L_\mathrm{p} - M$ and $L_\mathrm{s} - M$) represent the flux linkage differences (defined as leakage flux linkages), which can, for some designs, be negative (especially if $N_\mathrm{p} \neq N_\mathrm{s}$.

With the aforementioned inductance matrix, the inductances, voltage transfer ratios, and current transfer ratios can be expressed for short-circuit and open-circuit operations (cf. Fig. 2(b)):

$$L_\mathrm{oc,p} = L_\mathrm{p}, \qquad \frac{v_\mathrm{s}}{v_\mathrm{p}} = +k\sqrt{\frac{L_\mathrm{s}}{L_\mathrm{p}}}, \qquad \text{with } i_\mathrm{s} = 0, \tag{15}$$

$$L_\mathrm{oc,s} = L_\mathrm{s}, \qquad \frac{v_\mathrm{p}}{v_\mathrm{s}} = +k\sqrt{\frac{L_\mathrm{p}}{L_\mathrm{s}}}, \qquad \text{with } i_\mathrm{p} = 0, \tag{16}$$

$$L_\mathrm{sc,p} = \left(1-k^2\right) L_\mathrm{p}, \qquad \frac{i_\mathrm{s}}{i_\mathrm{p}} = -k\sqrt{\frac{L_\mathrm{p}}{L_\mathrm{s}}}, \qquad \text{with } v_\mathrm{s} = 0, \tag{17}$$

$$L_\mathrm{sc,s} = \left(1-k^2\right) L_\mathrm{s}, \qquad \frac{i_\mathrm{p}}{i_\mathrm{s}} = -k\sqrt{\frac{L_\mathrm{s}}{L_\mathrm{p}}}, \qquad \text{with } v_\mathrm{p} = 0. \tag{18}$$

The terminal behavior (cf. (12)) and the stored energy (cf. (13)) of the transformer can be represented with different equivalent circuits. The circuits shown in Fig. 1(b) are directly related to the inductance matrix. On the contrary, Fig. 14 depicts equivalent circuits,

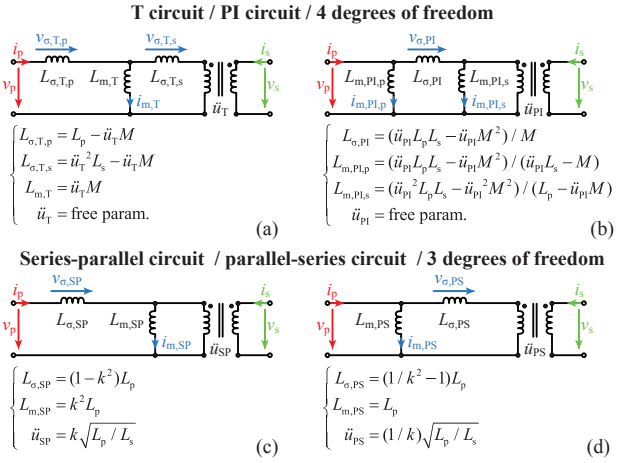

Fig. 14 Transformer (lossless) linear equivalent circuits. (a) T circuit, (b) PI circuit, (c) series-parallel circuit, and (d) parallel-series circuit. The circuits are referred to the primary side of the transformer.

which do not provide a direct insight on the magnetic flux linkages. The following important remarks can be given about the different equivalent circuits of transformers:

- All the presented equivalent circuits (cf. Fig. 1(b) and Fig. 14) model perfectly the terminal behavior and the stored energy.
- The equivalent circuits with more than three degrees of freedom (cf. Figs. 14(a) and (b)) are underdetermined and do not have a physical meaning, without accepting restrictive hypotheses [11].
- The turns ratio of the transformer, $N_\mathrm{p} : N_\mathrm{s}$, is not clearly defined for some transformer geometries (e.g. inductive power transfer coils) [47, 48]. This implies that the turns ratio is not always directly related to the flux linkages and to the magnetic parameters.
- The magnetizing and leakage fluxes cannot be spatially separated. In other words, it is not always possible to sort the magnetic field lines into leakage and magnetizing field lines [48].
- In a transformer, a phase shift is present between the primary and secondary currents, which originates from the modulation scheme, the load, and/or the losses. This implies that the distribution of the magnetic field lines is time-dependent [11, 48]. Therefore, the leakage and magnetizing flux linkages only have a clear interpretation for a lossless transformer during open-circuit and short-circuit operations.
- The magnetizing and leakage inductances are usually defined as the parallel and series inductances in the equivalent circuit, respectively. However, the values of these inductances depend on the chosen equivalent circuit (cf. Fig. 14) and, therefore, do not have a clear and/or unique physical interpretation. This also implies that the associated magnetizing current (i_m) and leakage voltage (v_σ) only represent virtual parameters, which are not directly measurable [11].

It can be concluded that only the equivalent circuits shown in Fig. 1(b) feature a clear physical interpretation and, therefore, should be preferred. The circuits with more than three degrees of freedom (cf. Figs. 14(a) and (b)) should be avoided since they are unnecessarily complex. The circuits depicted in Figs. 14(c) and (d) are interesting for designing transformers with high magnetic coupling factors as explained in Appendix D.

B Equivalent Circuit from Analytical Computations

The analytical methods are based on several assumptions (cf. Subsection 3.1). The inductances are accepted to scale quadratically with the number of turns. The inductances are extracted for $i_\mathrm{p} = 0 \vee i_\mathrm{s} = 0$

(the energy is confined inside the core and air gaps) and for $+N_\mathrm{p} i_\mathrm{p} = -N_\mathrm{s} i_\mathrm{s}$ (the energy is confined inside the winding window). Then, the following inductances can be extracted for a virtual 1 : 1 transformer:

$$L'_\mathrm{m} = 2\frac{W}{i_\mathrm{p}^2 N_\mathrm{p}^2} = 2\frac{W}{i_\mathrm{s}^2 N_\mathrm{s}^2}, \qquad \text{with } i_\mathrm{p} = 0 \vee i_\mathrm{s} = 0, \tag{19}$$

$$L'_\sigma = 2\frac{W}{i_\mathrm{p}^2 N_\mathrm{p}^2} = 2\frac{W}{i_\mathrm{s}^2 N_\mathrm{s}^2}, \qquad \text{with } +N_\mathrm{p} i_\mathrm{p} = -N_\mathrm{s} i_\mathrm{s}. \tag{20}$$

The equivalent circuit (cf. (12) and (14)) of the transformer is extracted such that the stored energy (cf. (13)) matches, which leads to

$$L_\mathrm{p} = N_\mathrm{p}^2 L'_\mathrm{m}, \qquad L_\mathrm{s} = N_\mathrm{s}^2 L'_\mathrm{m}, \tag{21}$$

$$M = N_\mathrm{p} N_\mathrm{s} \left(L'_\mathrm{m} - \frac{1}{2} L'_\sigma\right), \qquad k = 1 - \frac{1}{2}\frac{L'_\sigma}{L'_\mathrm{m}}. \tag{22}$$

The following expressions can be extracted for the open-circuit and short-circuit operations of the transformer:

$$L_\mathrm{oc,p} = N_\mathrm{p}^2 L'_\mathrm{m}, \qquad \frac{v_\mathrm{s}}{v_\mathrm{p}} = +k\frac{N_\mathrm{s}}{N_\mathrm{p}}, \qquad \text{with } i_\mathrm{s} = 0, \tag{23}$$

$$L_\mathrm{oc,s} = N_\mathrm{s}^2 L'_\mathrm{m}, \qquad \frac{v_\mathrm{p}}{v_\mathrm{s}} = +k\frac{N_\mathrm{p}}{N_\mathrm{s}}, \qquad \text{with } i_\mathrm{p} = 0, \tag{24}$$

$$L_\mathrm{sc,p} = N_\mathrm{p}^2 \left(\frac{1+k}{2}\right) L'_\sigma, \qquad \frac{i_\mathrm{s}}{i_\mathrm{p}} = -k\frac{N_\mathrm{p}}{N_\mathrm{s}}, \qquad \text{with } v_\mathrm{s} = 0, \tag{25}$$

$$L_\mathrm{sc,s} = N_\mathrm{s}^2 \left(\frac{1+k}{2}\right) L'_\sigma, \qquad \frac{i_\mathrm{p}}{i_\mathrm{s}} = -k\frac{N_\mathrm{s}}{N_\mathrm{p}}, \qquad \text{with } v_\mathrm{p} = 0. \tag{26}$$

C Equivalent Circuit from FEM Simulations

Different methods exist for extracting the magnetic equivalent circuit of a transformer from numerical simulations (e.g. FEM): integration of the magnetic flux, computation of the induced voltages, extraction of the energy, etc. The energy represents a numerically stable parameter which is easy to extract. Therefore, the energy is extracted for the following cases: $i_\mathrm{p} \neq 0 \wedge i_\mathrm{s} = 0$, $i_\mathrm{p} = 0 \wedge i_\mathrm{s} \neq 0$, and $+N_\mathrm{p} i_\mathrm{p} = -N_\mathrm{s} i_\mathrm{s}$. This last solution can be obtained by the superposition of the two first solutions. This leads to

$$L_\mathrm{p} = 2\frac{W}{i_\mathrm{p}^2}, \qquad \text{with } i_\mathrm{p} \neq 0 \wedge i_\mathrm{s} = 0, \tag{27}$$

$$L_\mathrm{s} = 2\frac{W}{i_\mathrm{s}^2}, \qquad \text{with } i_\mathrm{p} = 0 \wedge i_\mathrm{s} \neq 0, \tag{28}$$

$$M = \frac{W}{i_\mathrm{p} i_\mathrm{s}} - \frac{1}{2} L_\mathrm{p} \frac{i_\mathrm{p}}{i_\mathrm{s}} - \frac{1}{2} L_\mathrm{s} \frac{i_\mathrm{s}}{i_\mathrm{p}}, \qquad \text{with } +N_\mathrm{p} i_\mathrm{p} = -N_\mathrm{s} i_\mathrm{s}. \tag{29}$$

It should be noted that these expressions are general since no assumptions are required for the geometry, the turns ratio, the coupling factor, etc.

D Approximations for High Magnetic Coupling Factors

For a transformer with a high magnetic coupling factor ($k > 0.95$), the parameters of the equivalent circuits shown in Fig. 14 are converging together. Then, it is possible to define the transformer with the following parameters:

$$\begin{aligned} L_\sigma &\approx N_\mathrm{p}^2 L'_\sigma \approx L_\mathrm{sc,p} \approx L_\mathrm{sc,s} \frac{N_\mathrm{p}^2}{N_\mathrm{s}^2}, \\ &\approx 2L_{\sigma,\mathrm{T,p}} \approx 2L_{\sigma,\mathrm{T,s}} \approx L_{\sigma,\mathrm{PI}} \approx L_{\sigma,\mathrm{SP}} \approx L_{\sigma,\mathrm{PS}}, \end{aligned} \tag{30}$$

$$\begin{aligned} L_\mathrm{m} &\approx N_\mathrm{p}^2 L'_\mathrm{m} \approx L_\mathrm{oc,p} \approx L_\mathrm{oc,s} \frac{N_\mathrm{p}^2}{N_\mathrm{s}^2}, \\ &\approx L_{\mathrm{m,T}} \approx \frac{1}{2} L_{\mathrm{m,PI,p}} \approx \frac{1}{2} L_{\mathrm{m,PI,s}} \approx L_{\mathrm{m,SP}} \approx L_{\mathrm{m,PS}}, \end{aligned} \tag{31}$$

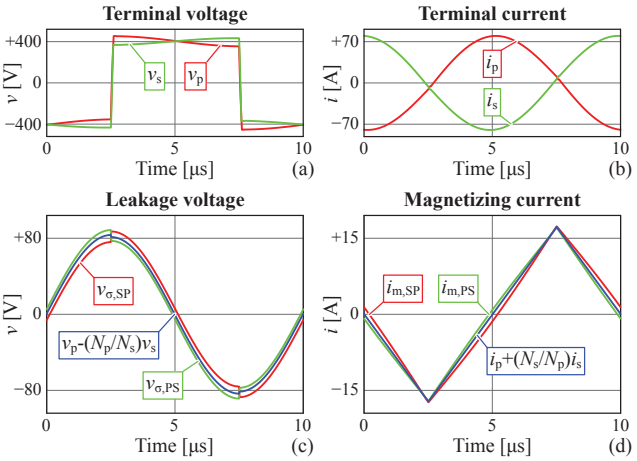

Fig. 15 Voltage and current waveforms for the considered MF transformer ($k = 0.986$, series-resonant LLC converter, cf. Fig. 2). (a) Terminal voltages, (b) terminal currents, (c) voltage across the leakage inductance, and (d) current through the magnetizing inductance. The equivalent circuits shown in Figs. 14(c) and (d) are considered and compared.

$$\ddot{u} \approx \frac{N_\mathrm{p}}{N_\mathrm{s}} \approx \ddot{u}_\mathrm{T} \approx \ddot{u}_\mathrm{PI} \approx \ddot{u}_\mathrm{SP} \approx \ddot{u}_\mathrm{PS}, \tag{32}$$

where L_σ is the leakage inductance, L_m the magnetizing inductance, and $\ddot{u}$ the voltage transfer ratio. These three parameters, which are nearly independent of the chosen equivalent circuit, are typically used for the design process of transformers.

Fig. 15 illustrates the leakage voltage and magnetizing current obtained with the equivalent circuits depicted in Figs. 14(c) and (d) for the considered MF transformer ($k = 0.986$, series-resonant LLC converter, cf. Fig. 2). It can be seen that the aforementioned approximations (cf. (31), (30), and (32)) are valid.

With these assumptions, a clear and unique definition of the leakage and magnetizing fluxes is achieved. The leakage field, which is linked to the magnetizing inductance (L_σ and v_σ), is located inside the winding window and is related to the load current (series inductance). The magnetizing field, which is linked to the magnetizing inductance (L_m and i_m), is located inside the core and air gaps and is related to the applied voltage (parallel inductance). During rated operating condition, the leakage and magnetizing magnetic fields feature 90° phase shift (cf. Fig. 15).

Acknowledgements This project is carried out within the frame of the Swiss Centre for Competence in Energy Research on the Future Swiss Electrical Infrastructure (SCCER-FURIES) with the financial support of the Swiss Innovation Agency.

References

1. M. Leibl, G. Ortiz, and J. W. Kolar, "Design and Experimental Analysis of a Medium Frequency Transformer for Solid-State Transformer Applications," *IEEE Trans. Emerg. Sel. Topics Power Electron.*, vol. 5, no. 1, pp. 110–123, 2017.
2. F. Kieferndorf, U. Drofenik, F. Agostini, and F. Canales, "Modular PET, Two-Phase Air-Cooled Converter Cell Design and Performance Evaluation with 1.7kV IGBTs for MV Applications," in *Proc. of the IEEE Applied Power Electronics Conf. and Expo. (APEC)*, Mar. 2016, pp. 472–479.
3. S. Zhao, Q. Li, and F. C. Lee, "High Frequency Transformer Design for Modular Power Conversion from Medium Voltage AC to 400V DC," in *Proc. of the IEEE Applied Power Electronics Conf. and Expo. (APEC)*, Mar. 2017, pp. 2894–2901.

4. T. Guillod, F. Krismer, and J. W. Kolar, "Electrical Shielding of MV/MF Transformers Subjected to High dv/dt PWM Voltages," in *Proc. of the IEEE Applied Power Electronics Conf. and Expo. (APEC)*, Mar. 2017, pp. 2502–2510.
5. J. Mühlethaler, "Modeling and Multi-Objective Optimization of Inductive Power Components," Ph.D. dissertation, ETH Zürich, 2012.
6. V. C. Valchev and A. Van den Bossche, *Inductors and Transformers for Power Electronics*. CRC press, 2005.
7. J. A. Ferreira, *Electromagnetic Modelling of Power Electronic Converters*. Springer Science & Business Media, 2013.
8. T. Guillod, R. Färber, F. Krismer, C. M. Franck, and J. W. Kolar, "Computation and Analysis of Dielectric Losses in MV Power Electronic Converter Insulation," in *Proc. of the IEEE Energy Conversion Congr. and Expo. (ECCE)*, Sep. 2016, pp. 1–8.
9. T. Guillod, F. Huber, J. Krismer, and J. W. Kolar, "Wire Losses: Effects of Twisting Imperfections," in *Proc. of the Workshop on Control and Modeling for Power Electronics (COMPEL)*, Jul. 2017, pp. 1–8.
10. K. Venkatachalam, C. R. Sullivan, T. Abdallah, and H. Tacca, "Accurate Prediction of Ferrite Core Loss with Nonsinusoidal Waveforms using only Steinmetz Parameters," in *Proc. of the IEEE Workshop on Computers in Power Electronics*, Jun. 2002, pp. 36–41.
11. H. Kleinrath, "Ersatzschaltbilder für Transformatoren und Asynchronmaschinen (in German)," *e&i*, vol. 110, no. 1, p. 68–74, 1993.
12. W. T. McLyman, *Transformer and Inductor Design Handbook*. CRC Press, 2004.
13. M. Kasper, R. M. Burkart, G. Deboy, and J. W. Kolar, "ZVS of Power MOSFETs Revisited," *IEEE Trans. Power Electron.*, vol. 31, no. 12, pp. 8063–8067, 2016.
14. F. C. Schwarz, "A Method of Resonant Current Pulse Modulation for Power Converters," *IEEE Trans. Ind. Electron.*, vol. 17, no. 3, pp. 209–221, 1970.
15. R. W. A. A. De Doncker, D. M. Divan, and M. H. Kheraluwala, "A Three-Phase Soft-Switched High-Power-Density DC/DC Converter for High-Power Applications," *IEEE Trans. Ind. Appl.*, vol. 27, no. 1, pp. 63–73, 1991.
16. N. Dai and F. C. Lee, "Edge Effect Analysis in a High-Frequency Transformer," in *Proc. of the IEEE Power Electronics Specialists Conf. (PESC)*, Jun. 1994, pp. 850–855.
17. M. Meinhardt, M. Duffy, T. O'Donnell, S. O'Reilly, J. Flannery, and C. O. Mathuna, "New Method for Integration of Resonant Inductor and Transformer-Design, Realisation, Measurements," in *Proc. of the IEEE Applied Power Electronics Conf. and Expo. (APEC)*, Mar. 1999, pp. 1168–1174.
18. L. M. R. Oliveira and A. J. M. Cardoso, "Leakage Inductances Calculation for Power Transformers Interturn Fault Studies," *IEEE Trans. Power Del.*, vol. 30, no. 3, pp. 1213–1220, 2015.
19. J. Muhlethaler, J. W. Kolar, and A. Ecklebe, "A Novel Approach for 3D Air Gap Reluctance Calculations," in *Proc. of the IEEE Energy Conversion Congr. and Expo. (ECCE Asia)*, May 2011, pp. 446–452.
20. A. Van den Bossche, V. C. Valchev, and R. Filchev, "Improved approximation for fringing permeances in gapped inductors," in *Proc. of the IEEE Industry Applications Conf.*, Oct. 2002, pp. 932–938.
21. Z. Ouyang, J. Zhang, and W. G. Hurley, "Calculation of Leakage Inductance for High-Frequency Transformers," *IEEE Trans. Power Electron.*, vol. 30, no. 10, pp. 5769–5775, 2015.
22. A. L. Morris, "The Influence of Various Factors upon the Leakage Reactance of Transformers," *Journal of the Institution of Electrical Engineers*, vol. 86, no. 521, pp. 485–495, 1940.
23. R. Doebbelin, M. Benecke, and A. Lindemann, "Calculation of Leakage Inductance of Core-Type Transformers for Power Electronic Circuits," in *Proc. of the IEEE International Power Electronics and Motion Control Conf. (PEMC)*, Sep. 2008, pp. 1280–1286.
24. Z. Ouyang, O. C. Thomsen, and M. A. E. Andersen, "The Analysis and Comparison of Leakage Inductance in Different Winding Arrangements for Planar Transformer," in *Proc. of the IEEE Conf. Power Electronics and Drive Systems (PEDS)*, Nov. 2009, pp. 1143–1148.
25. A. M. Urling, V. A. Niemela, G. R. Skutt, and T. G. Wilson, "Characterizing High-Frequency Effects in Transformer Windings - A Guide to Several Significant Articles," in *Proc. of the IEEE Applied Power Electronics Conf. and Expo. (APEC)*, Mar. 1989, pp. 373–385.
26. J. Mühlethaler and J. W. Kolar, "Optimal Design of Inductive Components Based on Accurate Loss and Thermal Models," in *Tutorial at the IEEE Applied Power Electronics Conf. and Expo. (APEC)*, Feb. 2012.
27. R. Doebbelin, C. Teichert, M. Benecke, and A. Lindemann, "Computerized Calculation of Leakage Inductance Values of Transformers," *Piers Online*, vol. 5, no. 8, pp. 721–726, 2009.
28. G. AlLee and W. Tschudi, "Edison Redux: 380 Vdc Brings Reliability and Efficiency to Sustainable Data Centers," *IEEE Power Energy Mag.*, vol. 10, no. 6, pp. 50–59, 2012.
29. A. Pratt, P. Kumar, and T. V. Aldridge, "Evaluation of 400V DC Distribution in Telco and Data Centers to Improve Energy Efficiency," in *Proc. of the IEEE Telecommunications Energy Conference (INTELEC)*, Oct. 2007, pp. 32–39.
30. R. M. Burkart and J. W. Kolar, "Comparative η-ρ-σ Pareto Optimization of Si and SiC Multilevel Dual-Active-Bridge Topologies with Wide Input Voltage Range," *IEEE Trans. Power Electron.*, vol. 32, no. 7, pp. 5258–5270, 2017.
31. K. J. Binns and P. J. Lawrenson, *Analysis and Computation of Electric and Magnetic Field Problems*. Elsevier, 1973.
32. D. Leuenberger and J. Biela, "Accurate and Computationally Efficient Modeling of Flyback Transformer Parasitics and their Influence on Converter Losses," in *Proc. of the European Conf. on Power Electronics and Applications (EPE)*, Sep. 2015, pp. 1–10.
33. M. Eslamian and B. Vahidi, "New Methods for Computation of the Inductance Matrix of Transformer Windings for Very Fast Transients Studies," *IEEE Trans. Power Del.*, vol. 27, no. 4, pp. 2326–2333, 2012.
34. M. Lambert, F. Sirois, M. Martinez-Duro, and J. Mahseredjian, "Analytical Calculation of Leakage Inductance for Low-Frequency Transformer Modeling," *IEEE Trans. Power Del.*, vol. 28, no. 1, pp. 507–515, 2013.
35. G. R. Skutt, F. C. Lee, R. Ridley, and D. Nicol, "Leakage Inductance and Termination Effects in a High-Power Planar Magnetic Structure," in *Proc. of the IEEE Applied Power Electronics Conf. and Expo. (APEC)*, Feb. 1994, pp. 295–301.
36. I. J. Bahl, *Lumped Elements for RF and Microwave Circuits*, ser. Artech House Microwave Library. Artech House, 2003.
37. S. S. Rao, *The Finite Element Method in Engineering*. Elsevier Science, 2011.
38. I. M. Sobol, *A Primer for the Monte Carlo Method*. CRC press, 1994.
39. F. Scholz, "Tolerance Stack Analysis Methods," *Research and Technology: Boeing Information*, pp. 1–44, 1995.
40. L. C. Andrews, *Special Functions of Mathematics for Engineers*, ser. Oxford Science Publications. SPIE Optical Engineering Press, 1992.
41. Agilent Technologies, "Agilent 4294A Precision Impedance Analyzer, Operation Manual," Feb. 2003.
42. ed-k, "Power Choke Tester DPG10 – Series," Feb. 2017.
43. J. G. Hayes, N. O'Donovan, M. G. Egan, and T. O'Donnell, "Inductance Characterization of High-Leakage Transformers," in *Proc. of the IEEE Applied Power Electronics Conf. and Expo. (APEC)*, Feb. 2003, pp. 1150–1156.
44. omicron lab, "Bode 100, User Manual," Feb. 2010.
45. ——, "B-WIC & B-SMC, Impedance Test Adapters," Feb. 2014.
46. A. Quarteroni and F. Saleri, *Scientific Computing with MATLAB*, ser. Texts in Computational Science and Engineering. Springer Berlin Heidelberg, 2012.
47. W. G. Hurley, M. C. Duffy, J. Zhang, I. Lope, B. Kunz, and W. H. Wölfle, "A Unified Approach to the Calculation of Self- and Mutual-Inductance for Coaxial Coils in Air," *IEEE Trans. Power Electron.*, vol. 30, no. 11, pp. 6155–6162, 2015.
48. R. Bosshard, T. Guillod, and J. W. Kolar, "Electromagnetic Field Patterns and Energy Flux of Efficiency Optimal Inductive Power Transfer Systems," *Electrical Engineering (Springer)*, vol. 99, no. 3, pp. 969–977, 2017.